SECURITY INFORMATION
CONFIDENTIAL
UNCLASSIFIED

C.2
6
Copy
RM E52D11

NACA RM E52D11

NACA

RESEARCH MEMORANDUM

INVESTIGATION OF HEAT-TRANSFER COEFFICIENTS IN AN AFTERBURNER

By William K. Koffel and Harold R. Kaufman

Lewis Flight Propulsion Laboratory
Cleveland, Ohio

CLASSIFICATION CHANGED
To UNCLASSIFIED UNAVAILABLE
By authority of TPA #39 Date Jan 12 1961
xdj-jw

CLASSIFIED DOCUMENT

This material contains information affecting the National Defense of the United States within the meaning of the espionage laws, Title 18, U.S.C., Secs. 793 and 794, the transmission or revelation of which in any manner to an unauthorized person is prohibited by law.

NATIONAL ADVISORY COMMITTEE
FOR AERONAUTICS

WASHINGTON
June 27, 1952

CONFIDENTIAL
UNCLASSIFIED

UNCLASSIFIED

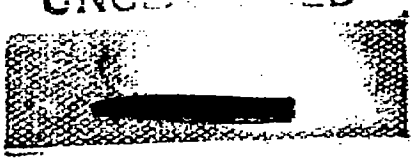

NASA Technical Library
3 1176 01435 5839

NATIONAL ADVISORY COMMITTEE FOR AERONAUTICS

RESEARCH MEMORANDUM

INVESTIGATION OF HEAT-TRANSFER COEFFICIENTS IN AN AFTERBURNER

By William K. Koffel and Harold R. Kaufman

2571

SUMMARY

The relative importance of the heat-transfer modes in an experimental afterburner were evaluated. The convective heat-transfer coefficients near the combustion-chamber outlet were determined and the effects of three radial distributions of afterburner fuel across the turbine-outlet annulus on the convective heat-transfer coefficient were examined.

The combined heat-transfer coefficient for convection and radiation from the combustion gas to the combustion-chamber wall and the over-all heat-transfer coefficient were practically unaffected by the combustion-gas temperature level, but they varied, in similar manner, along the combustion-chamber length. However, the convective heat-transfer coefficient without afterburning was practically constant along the combustion-chamber length.

The heat transferred from the combustion gas to the combustion chamber wall by nonluminous radiation varied from about one-fifth to one-third of the total heat transferred by convection and radiation, depending on the radial distribution of fuel across the turbine-outlet annulus.

INTRODUCTION

Current afterburners require some form of cooling system in order that the combustion-chamber wall temperatures will not exceed safe values. Most afterburners are cooled at present by air flowing through an annular cooling passage surrounding the combustion chamber. The design of such annular cooling systems has been based upon heat-transfer data that are available in the general literature for nonluminous radiation and for forced convection in long tubes or over flat plates. Such heat-transfer data may not apply, however, to the convective heat-transfer coefficients in afterburner combustion chambers because of the relatively small length-diameter ratios of afterburners or because the velocity and temperature profiles usually differ greatly from those existing in the setups used to obtain heat-transfer data in tubes and over flat plates. In addition, the effects of luminous radiation are not known, and information on the relative importance of the heat-transfer processes in actual afterburners is not found in the literature.

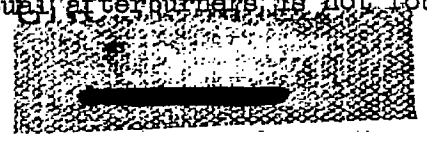

UNCLASSIFIED

Accordingly, the Lewis laboratory of the NACA designed and extensively instrumented an experimental afterburner for an investigation of the cooling characteristics and temperature profiles in an actual afterburner cooled by air flowing through an annular cooling passage. The experimental investigation provided data for the establishment of an empirical cooling correlation relating the combustion-chamber wall temperatures near the burner outlet to known engine performance parameters, and for the determination of the relative importance of the convective and radiative heat-transfer processes in an afterburner. Reference 1 tabulates the data of this investigation and graphically shows the effects of exhaust-gas temperature level, combustion-gas flow, and radial distribution of afterburner fuel across the turbine-outlet annulus on the temperature profiles of the combustion gas and of the combustion-chamber wall. The variation of wall temperatures with the inlet cooling-air temperature and the mass flow ratio of cooling air to the combustion gas are also shown. An empirical cooling correlation is established from the data of this afterburner in reference 2. The correlation equation provides a rapid and convenient means of calculating the wall temperatures for any combination of combustion-gas flow, combustion-gas temperature, cooling-air flow, and cooling-air temperature without recourse to the fundamentals of the heat-transfer processes.

This report presents the heat-transfer coefficients for the combustion chamber and provides a better insight into the magnitudes and variations of the heat-transfer processes in an afterburner. The data in this report were obtained with nonluminous combustion, although some luminosity may be produced under different conditions in other afterburners.

Because only convection and nonluminous radiation were present during this investigation and because the nonluminous radiation can be calculated with reasonable accuracy from the data of reference 3, the convective heat-transfer coefficient has been determined and is presented in nondimensional form on the usual Nusselt-Reynolds number plot. The resulting correlations for three different radial distributions of fuel across the turbine-outlet annulus are compared with the correlation of convective heat-transfer coefficients for turbulent flow in long tubes. The variations of the over-all heat-transfer coefficient and of the combined coefficient for convection and radiation from the combustion gas to the combustion-chamber wall are shown for various stations along the burner length and are discussed. The heat-transfer coefficients in the cooling passage are not presented herein because of the widespread availability of such information in the heat-transfer literature.

2571

2571

APPARATUS AND PROCEDURE

Test Installation

A schematic drawing of the experimental afterburner used in this cooling investigation is shown in figure 1. The cylindrical combustion chamber was fabricated of 1/16-inch-thick Inconel and had a length of 5 feet from the flame holder center line to the exhaust nozzle inlet and an inside diameter of 26 inches. The annular cooling passage was 1/2 inch in height and was insulated with 1 inch of refractory cement. The flame holder had a single V-gutter with sinusoidal corrugations on the trailing edge. The V-gutter had a mean diameter of 18 inches, a mean width across the corrugations of $1\frac{3}{4}$ inches, and an included angle of 35°. The blockage at the downstream face of the flame holder was about 23 percent and the velocity at the flame holder under the conditions of the investigation was approximately 480 feet per second.

Twelve radial fuel-spray bars were equally spaced circumferentially in a plane 8.75 inches downstream of the turbine flange and 13.25 inches upstream of the flame-holder center line. Three different configurations (12 spray bars per configuration) of spray bars were used to study the effects of various radial fuel distributions on the correlation of the convective heat-transfer coefficients for the gas side of the combustion-chamber wall. Configuration A (fig. 2) produced a nearly uniform fuel distribution. Configuration B increased the fuel concentration near the combustion-chamber wall and decreased the fuel flow in the center of the combustion chamber. Configuration C concentrated more fuel at the center and decreased the concentration near the combustion-chamber walls.

Instrumentation

Extensive instrumentation was provided at six longitudinal stations (fig. 1) B, C, D, E, F, and G, with four of these stations, C, D, E, and F, having six circumferential groups of instrumentation. (Details of the instrumentation are given in reference 1.)

Because of the large number of thermocouples, four flight recorders were used to reduce the recording time while maintaining equilibrium conditions. The transverse temperature profiles of the combustion gas at station F were obtained qualitatively by means of a vertical rake having seven sonic-flow-orifice temperature probes (reference 4). In this report, the temperatures of the combustion-chamber wall and of the cooling air at each station are arithmetic averages of the respective temperatures measured at six equally spaced positions around the circumference of the burner. The estimated over-all accuracies of the individual temperature measurements are as follows:

Wall temperature, °F . . . . . ±15
Cooling air, °F . . . . . ±10
Exhaust-gas temperature, °F . . . . . ±50
Transverse temperature profile, °F . . . . . ±150

Range of Test Data

The afterburner used in this investigation incorporated the best available experimental design information for high performance. Preliminary tests were conducted on a similar uninstrumented afterburner to confirm that the afterburner configuration for this investigation had high performance and good operating characteristics over a wide range of fuel-air ratio and altitude. The final geometry of the turbine-diffuser inner cone and flame holder in combination with the fuel-spray bars producing approximately uniform distribution of fuel across the turbine annulus is designated configuration A. The various combinations of conditions investigated are tabulated in the following table:

Configuration	Altitude (ft)	Exhaust-gas temperature $T_{g,1}$ (°R)	Combustion-gas flow W_g (lb/sec)	Mass flow ratio W_a/W_g	Inlet cooling-air temperature $T_{a,0}$ (°R)
A	30,000	3060	22.1	0.0672 to .1872	500 to 1587
	30,000	3240	22.2	0.1002 to .1917	500 to 1222
	30,000	3435	22.3	0.0953 to .1796	502 to 1408
	40,000	3265	13.8	0.1440	528 to 1340
	30,000	3825	22.8	0.1374 to .1906	515
B	30,000	3215	22.2	0.0985 to .1891	495 to 1223
C	30,000	3235	22.3	0.1420	524 to 1450
	30,000	3764	22.4	0.1912	524

[redacted]

The mass flow rate of cooling air W_a and the inlet cooling-air temperature $T_{a,0}$ were systematically varied while all other quantities were held constant.

Configurations A, B, and C differed only in the radial distribution of fuel across the turbine annulus. The data presented are for a simulated flight Mach number of 0.52, rated engine speed, and an afterburner-inlet (turbine-outlet) temperature of 1633 $\pm$12° R. The data were obtained at combustion-chamber static pressures of 750 to 1400 pounds per square foot absolute. The fuel-air ratios ranged from 0.031 to 0.066, and afterburner combustion efficiencies were about 0.90 to 0.95.

2571

ANALYSIS

Frequent observations were made of the flame during this investigation, both into the combustion chamber from the exhaust end and from the side of the exhaust jet. The flame was translucent and varied for the range of test conditions from a light blue violet to turquoise with no yellow luminosity. Because the flame was nonluminous (see reference 5 for the definitions of nonluminous and luminous radiation), heat transfer from the combustion gas to the combustion chamber walls was due to forced convection and nonluminous radiation only, in this afterburner. However, luminous radiation has been observed in other afterburners during actual take-off conditions and in laboratory investigations of combustion at combustion-chamber pressures of approximately two atmospheres

The following analysis is based on one-dimensional flow. All temperatures are considered to be total temperatures because the thermocouples used had recovery factors of about 0.85 and the ratio of static to total temperatures was always greater than 0.95 (Mach numbers of 0.5 or less). Negligible errors result in the calculation of the radiant heat transfer even though radiation is a function of the static temperature. It is also assumed that radiation gained by the wall from a higher temperature region downstream is balanced by the radiation lost to the cooler region upstream of a given station. In effect, this assumption places radiation on a one-dimensional basis like the convective heat transfer so that the temperature differences at a station can be used instead of log mean temperature differences over a finite length of the combustion chamber.

Calculation of dq/dA. - The heat flux per unit area of the combustion-chamber wall was calculated from the equation

$$\frac{dq}{dA} = 3600 \frac{W_a \, c_{p,a}}{\pi D} \frac{dT_a}{dx} \qquad (1)$$

(All symbols are defined in the appendix.) The derivative dT_a/dx for each station along the burner length was measured from faired curves of

[redacted]

cooling-air temperature against the distance downstream of the flame holder (fig. 3).

Calculation of heat-transfer coefficients. - The heat flux per unit area of the combustion-chamber wall at a given station is also given by

$$\frac{dq}{dA} = U(T_g - T_a) \tag{2}$$

or the over-all heat-transfer coefficient U is

$$U = \frac{dq/dA}{T_g - T_a} \tag{3}$$

The heat transfer per unit area of the wall by forced convection and nonluminous radiation from the combustion gas is

$$\frac{dq}{dA} = h_g(T_g - T_w) + \sigma \varepsilon_w' \left(\varepsilon_g T_g^4 - \alpha_g T_w^4\right) \tag{4}$$

Rearranging equation (4) gives the combined heat-transfer coefficient

$$h_g + h_{r,g} = \frac{dq/dA}{T_g - T_w} \tag{5}$$

where

$$h_{r,g} = \sigma \varepsilon_w' \frac{\left(\varepsilon_g T_g^4 - \alpha_g T_w^4\right)}{T_g - T_w} \tag{6}$$

and is the heat-transfer coefficient for nonluminous radiation. When the emissivity ε_g and the absorptivity α_g are known, the convective heat-transfer coefficient can be obtained from equation (4) as

$$h_g = \frac{dq/dA - \sigma \varepsilon_w' \left(\varepsilon_g T_g^4 - \alpha_g T_w^4\right)}{T_g - T_w} \tag{7}$$

The emissivity and absorptivity were calculated for station F, from charts in reference 3, where the combustion process is complete enough that the partial pressures of the carbon dioxide and of the water vapor in the combustion gas can be computed from the total fuel-air ratio and the local static pressure in the combustion chamber. The equivalent beam length for radiation was taken as 0.85 times the combustion-chamber diameter.

In the correlation of the convective heat-transfer coefficient, the physical properties of air were used in the Nusselt number, Reynolds number, and Prandtl number. The physical properties were evaluated at

2571

the film temperature T_f, which is the arithmetic mean of the bulk gas temperature T_g at the wall temperature T_w. The viscosity and specific heat at constant pressure were taken from table II of reference 6. Thermal conductivity was assumed to be proportional to the square root of the film temperature as in reference 7, with the constant of proportionality being evaluated at a temperature of 500° R.

2571

Longitudinal distribution of combustion gas temperature. - Heat transfer depends on temperature differences and hence upon a knowledge of the temperatures of the combustion gas, combustion chamber wall, and cooling air. The longitudinal distribution of combustion-gas bulk temperature was not measured directly in this investigation so that it was necessary to compute the combustion-gas temperatures at each station from an equation relating the combustion gas to the known temperatures at the burner inlet and at the exhaust-nozzle outlet. It was found in reference 2 that the longitudinal distribution of static pressure in the combustion chamber of this investigation could be calculated quite accurately when the longitudinal distribution of combustion-gas bulk temperature was given by the equation

$$\frac{T_{g,x}-T_{g,0}}{T_{g,1}-T_{g,0}} = \sin\frac{\pi}{2}\frac{x}{L} \tag{8}$$

Equation (8) is therefore used in this report.

RESULTS AND DISCUSSION

The convective heat-transfer coefficient at station F is presented first and the effects of radial distribution of afterburner fuel on the convective heat-transfer coefficient are discussed. The effects of several parameters on the combined heat-transfer coefficient for convection and radiation on the gas side of the wall and on the over-all heat-transfer coefficient are then shown to provide a better insight into the variation and magnitudes of the heat-transfer processes.

Convective Heat-Transfer Coefficient at Station F

Configuration A. - The convective heat-transfer coefficient h_g at station F was calculated from equation (7) and is plotted in the usual non-dimensional manner in figure 4. The abscissa is a modified Reynolds number $\rho_f \frac{V_b D}{\mu_f}$ which is equivalent to $\frac{GD}{\mu_f}\frac{T_g}{T_f}$, where the temperature ratio corrects the density to film conditions. The effects of combustion-gas temperature level (fuel-air ratio) are random and within the scatter

of the data. For configuration A the data points lie within ±0.15 of the line representing the equation

$$\frac{h_g D}{k_f} = 0.034 \left(\rho_f \frac{V_b D}{\mu_f}\right)^{0.8} \left(\frac{c_{p,f}\, \mu_f}{k_f}\right)^{0.4} \left(\frac{L}{D}\right)^{-0.1} \qquad (9)$$

Equation (9) gave the best correlation of experimental convective heat-transfer coefficients in reference 7 for subsonic flow of air in smooth tubes at high surface and fluid temperatures.

The transverse temperature profiles at station F for configuration A are shown in figure 5 for a range of combustion-gas temperatures. The shape of these profiles approached the shape occurring with fully developed turbulent flow, especially as the temperature level was increased, and probably contributed to the good agreement between the heat-transfer coefficients of configuration A and equation (9).

Effect of radial fuel distribution. - The effects of two extremes in the radial distribution of afterburner fuel on the convective heat-transfer coefficient are shown in figure 6 for a modified Reynolds number of 540,000. The Nusselt number, and consequently the convective heat-transfer coefficient h_g, for configuration B was about 53 percent higher than for configuration A, whereas the Nusselt number was about 40 percent lower for configuration C. This wide range in Nusselt number, or in the convective heat-transfer coefficient, is attributed to the differences in the transverse profiles of the combustion-gas temperature and consequently in the temperature gradients in the boundary layer for each fuel distribution because the bulk temperature and wall temperature were maintained at 3000° and 1510° R, respectively, for configurations B and C.

The transverse temperature profiles at station F for configurations B and C are shown in figure 7 for a combustion gas temperature of 3000° R. The fuel distributions of configurations B and C resulted in quite different temperature profiles than for fully developed turbulent flow. Configuration B is characterized by high gas temperatures near the wall and configuration C by lower gas temperatures near the wall. Thus fuel distribution has a powerful influence on the transverse temperature profile and consequently on convective heat transfer. The vertical scatter in the data in figure 6 may be caused by small variations in the fuel distribution. Configuration A gave high performance with good operating characteristics over a wide range of operating conditions, whereas configurations B and C had poor performance and undesirable operating or cooling characteristics. The simultaneous achievement of high performance and good operating characteristics requires a certain

2571

combination of fuel distribution and flame-holder design. The latitude of these combinations is relatively small and in view of the results of figure 6, it is believed that equation (9) can be used to calculate the convective heat-transfer coefficient near the combustion-chamber outlet in other high-performance afterburners.

The transverse profiles of total pressure at station F were examined to determine whether the pressure profiles could be used in foretelling the temperature profiles for the purpose of adjusting the constant of proportionality in equation (9) for various fuel distributions. The ratio of the total pressure to the static pressure at the wall is shown against the burner diameter in figure 8. The profiles give no hint of the differences in the temperature profiles. Some correspondence might, however, have been found if the static pressure profiles had been available.

2571

Combined Heat-Transfer Coefficient

The variation of the combined heat-transfer coefficient $h_g + h_{r,g}$ with the difference between the temperatures of the combustion gas and of the combustion-chamber wall $T_g - T_w$ is shown in figure 9 for stations C to F. The data points are for an inlet cooling-air temperature of about 520° R with a varying mass-flow ratio (tailed symbols) and for a mass-flow ratio of about 0.144 and varying inlet cooling-air temperature (no tails). A single curve resulted for each station within the scatter of the data for the range of combustion-gas temperatures investigated when the combustion gas flow was constant. The combined heat-transfer coefficient increased at a decreasing rate as the temperature difference $T_g - T_w$ was increased. Decreasing the flow rate of combustion gas resulted in similar curves of decreased value for each station (fig. 9).

The faired curves of the combined heat-transfer coefficient $h_g + h_{r,g}$ from figure 9 are cross plotted in figure 10 with the temperature difference $T_g - T_w$ as a parameter and a combustion-gas flow of 22.3 pounds per second. Typical longitudinal distributions of the combined coefficient $h_g + h_{r,g}$ are shown by operating lines for typical longitudinal distributions of combustion-chamber wall temperature corresponding to combustion-gas temperatures at station F of 3000° and 3500° R. The operating lines are similar in shape and have approximately the same magnitude. Along the operating lines the combined coefficient $h_g + h_{r,g}$ decreased from about 22 to a minimum of about 17 Btu per hour per square foot per degree at a distance 26 inches downstream of the flame holder, after which the value increased to about 26 at station F. Nonluminous

radiation is slight during the initial decrease of $h_g + h_{r,g}$ so that the trend of the operating line primarily represents the variation of h_g with distance downstream of the flame holder. The combustion chamber may be compared with the entrance region of a large pipe, where the convective heat-transfer coefficient is known to decrease rapidly in the first diameter of length and less rapidly in the succeeding diameters until fully developed turbulent flow is established. The "entrance" effect was accentuated in the afterburner of this investigation because the bluff inner cone resulted in a higher mass flow per unit area (or Reynolds number) at the burner inlet than at the burner outlet. The increase in $h_g + h_{r,g}$ in the last half of the combustion chamber is due to the increases in the nonluminous radiation and in the convective heat-transfer coefficient as the temperature gradients near the wall increase.

Examination of the convective heat-transfer coefficient for nonafterburning data points revealed that the coefficient h_g (negligible nonluminous radiation) was practically constant along the combustion-chamber length. The average value of h_g without afterburning in this particular afterburner was 23.5 Btu per hour per square foot per degree for a combustion gas flow rate of 22.3 pounds per second. Thus, without afterburning, the coefficient h_g exceeded the afterburning value of the combined coefficient $h_g + h_{r,g}$ for configuration A for the first 44 inches downstream of the flame holder (see fig. 10). This unusual effect is attributed to the persistance of a low-velocity core in the wake of the bluff inner cone, without afterburning as far downstream as station F which resulted in a higher effective mass flow per unit area (or Reynolds number) near the wall. The low velocity core is illustrated by the transverse pressure profiles of figure 11. The transverse variation of the ratio of total pressure $P_{g,F}$ to the static pressure $p_{g,F}$ at the wall is shown for a range of burner inlet temperatures from 1182° (nonafterburning) to 1636° R. The pressure ratio $P_{g,F}/p_{g,F}$ is higher near the walls and reaches a minimum at the center. The minimum is lowest for nonafterburning and increased nearly linearly as the burner-inlet temperature was increased to 1636° R. Thus the low-velocity wake of the inner cone without afterburning maintained the effectively high mass flow per unit area (or Reynolds number near the burner wall) existing at the burner inlet. The effective mass flow per unit area at station F was decreased, however, with afterburning by the expansion of the burning gas into the center of the burner.

Over-All Heat-Transfer Coefficient

The variation of the over-all heat-transfer coefficient U across the combustion chamber wall, with the mass flow ratio W_a/W_g is shown

2571

in figure 12 for configuration A and a combustion-gas flow of 22.3 pounds per second. At each station, the coefficient U increased gradually with decreasing rate as the mass-flow ratio was increased. The reciprocal of the combined heat-transfer coefficient is the controlling resistance to heat flow and thus makes the over-all heat-transfer coefficient less sensitive to changes in mass-flow ratios approaching 0.20.

The over-all heat-transfer coefficient is shown in figure 13 as a function of the difference between the temperatures of the combustion gas and of the combustion-chamber wall. Figure 13 is similar to figure 9 for the combined heat-transfer coefficient. The data points are for an inlet cooling-air temperature of about 520° R with a varying mass-flow ratio (tailed symbols) and for a mass-flow ratio of about 0.144 and varying inlet cooling-air temperature (no tails). A single curve resulted, within the scatter of the data, for a constant combustion-gas flow over the range of combustion-gas temperatures investigated. The over-all heat-transfer coefficient increased gradually with decreasing rate as the temperature difference $T_g - T_w$ was increased. Decreasing the combustion-gas flow resulted in similar curves of lower value for each station (fig. 13).

2571

A cross plot of the faired curves of U from figure 13 for a combustion-gas flow of 22.3 pounds per second against distance downstream of the flame holder is presented in figure 14. Typical longitudinal variation of U is shown by operating lines for typical longitudinal variations of wall temperature corresponding to combustion-gas temperatures at station F of 3000° and 3500° R. The operating lines are similar in shape and have approximately the same magnitude. The longitudinal variation of U is quite similar to that of the combined heat-transfer coefficient $h_g + h_{r,g}$ because the reciprocal of the latter coefficient is the controlling resistance to heat transfer across the combustion-chamber wall.

Relative Magnitudes of Convective and Radiant Heat Transfer

Typical values of the heat transfer coefficients have been tabulated for station F at an average wall temperature $T_{w,F}$ of 1510° R in the following table:

Configuration	Combustion-gas flow (lb/sec)	Heat-transfer coefficients (Btu/(hr)(sq ft)(°R))			
		h_g	$h_{r,g}$	$h_g+h_{r,g}$	U
A	22.3	18.5	6.0	24.5	17.5
A	13.8	12.3	4.2	16.5	11.5
B	22.3	27.0	6.0	33.0	21.0
C	22.3	10.6	5.8	16.4	12.5

2571

The changes in radial distribution of fuel affected the ratio of radiant to convective heat transfer. The heat transferred by nonluminous radiation was about one-fourth, one-fifth, and one-third of the total heat transferred to the wall, for configurations A, B, and C, respectively. The ratio of the over-all heat-transfer coefficient to the combined heat-transfer coefficient was affected only slightly by variations in the radial distribution of fuel. The over-all heat-transfer coefficient was approximately 0.7 of the combined coefficient for the three fuel distributions tested.

CONCLUDING REMARKS

The heat-transfer coefficient h_g for convection between the combustion gas and the combustion-chamber wall for the fuel distribution providing the best afterburner performance was correlated within ±15 percent by a modified correlation equation for subsonic flow of air in smooth tubes at high surface and fluid temperatures.

The investigation of the variation of radial distribution of afterburner fuel across the turbine-outlet annulus gave values for the convective heat-transfer coefficient that were 53 percent higher to 40 percent lower than the convective coefficient h_g for the best fuel distribution, but performance was poor. The simultaneous achievement of high performance and good operating characteristics requires a certain combination of fuel distribution and flame-holder design. The latitude of these combinations is relatively small so that it is believed that the correlation presented for the convective heat-transfer coefficient is generally applicable to the combustion-chamber outlet for other high-performance afterburners.

The combined heat-transfer coefficient for convection and radiation from the combustion gas to the wall and the over-all heat-transfer coefficient decreased to a minimum about halfway along the combustion-chamber

length and then increased toward the combustion-chamber outlet. For typical longitudinal distributions of combustion-chamber wall temperature, the magnitudes and longitudinal variation of the combined heat-transfer coefficient and the over-all heat-transfer coefficient were practically unaffected by the combustion-gas temperature level for the same combustion-gas flow.

The convective heat-transfer coefficient without afterburning was practically constant along the combustion chamber length, with a value that corresponded to the combined heat-transfer coefficient for convection and radiation at the burner inlet with afterburning.

In the afterburner of this investigation, heat was transferred from the combustion gas to the combustion-chamber walls by forced convection and nonluminous radiation only. The heat transferred by nonluminous radiation varied from about one-fifth to one-third of the total heat transferred by convection and radiation, depending on the radial distribution of fuel across the turbine-outlet annulus.

Lewis Flight Propulsion Laboratory
National Advisory Committee for Aeronautics
Cleveland, Ohio

2571

APPENDIX - SYMBOLS

The following symbols are used in this report:

A	heat transfer surface area, sq ft
c_p	specific heat at constant pressure, Btu/(lb)(°R)
D	combustion-chamber diameter, ft
G	mass velocity of combustion gas, lb/(sec)(sq ft)
h	heat-transfer coefficient, Btu/(hr)(sq ft)(°R)
k	thermal conductivity, Btu/(hr)(ft)(°R)
L	distance from flame-holder center line to exhaust-nozzle exit, ft (6.21 ft for this afterburner)
P	total pressure, lb/sq ft abs
p	static pressure, lb/sq ft abs
q	heat flow rate, Btu/hr
T	bulk total temperature or wall temperature, °R
T_f	film temperature, arithmetic mean of bulk and wall temperatures, °R
U	over-all heat-transfer coefficient, Btu/(hr)(sq ft)(°R)
V_b	velocity of flow based on bulk temperature, T_g, ft/sec
W	flow rate, lb/sec
x	distance downstream of flame-holder center line, ft
α	adsorptivity, dimensionless
ε	emissivity, dimensionless
ε'_w	pseudoemissivity of the wall, $\frac{1+\varepsilon_w}{2}$ (0.9 for this afterburner)
μ	absolute viscosity, lb/ft sec
ρ	weight density of combustion gas, lb/cu ft

2571

[redacted]

2571

σ	Stefan-Boltzman constant, 0.173×10^{-8}, Btu/(hr)(sq ft)($^{\circ}$R)^4
$\frac{hD}{k}$	Nusselt number
$\frac{c_p \mu}{k}$	Prandtl number
$\rho \frac{VD}{\mu}$	Reynolds number

Subscripts:

a	cooling air
B,C,D,E,F,G	stations along the combustion-chamber length
f	property evaluated at film temperature
g	gas or combustion chamber
r	radiation
w	combustion-chamber wall
x	variable station
0	flame-holder center line
1	exhaust-nozzle exit

REFERENCES

1. Koffel, William K., and Kaufman, Harold R.: Cooling Characteristics of an Experimental Tail-Pipe Burner with an Annular Cooling-Air Passage. NACA RM E51K23, 1952.

2. Koffel, William K., and Kaufman, Harold R.: Empirical Cooling Correlation for an Experimental Afterburner with an Annular Cooling Passage. NACA RM E52C13, 1952.

3. McAdams, William H.: Heat Transmission. Chap. III by Hoyt C. Hottel, McGraw-Hill Book Co., Inc., (New York), 1942, pp. 45-86.

4. Blackshear, Perry L., Jr.: Sonic-Flow-Orifice Temperature Probe for High-Gas-Temperature Measurements. NACA TN 2167, 1950.

5. Thring, M. W.: Research on flame radiation - The plan of an attempt to fill in an important gap in fuel technology. Fuel, vol. XXIX, no. 8, Aug. 1950, pp. 173-177.

6. Keenan, Joseph H., and Kaye, Joseph: Gas Tables. John Wiley & Sons, Inc., New York, 1948.

7. Humble, Leroy V., Lowdermilk, Warren H., and Desmon, Leland G.: Measurement of Average Heat-Transfer and Friction Coefficients for Subsonic Flow of Air in Smooth Tubes at High Surface and Fluid Temperatures. NACA Rep. 1020, 1951.

2571

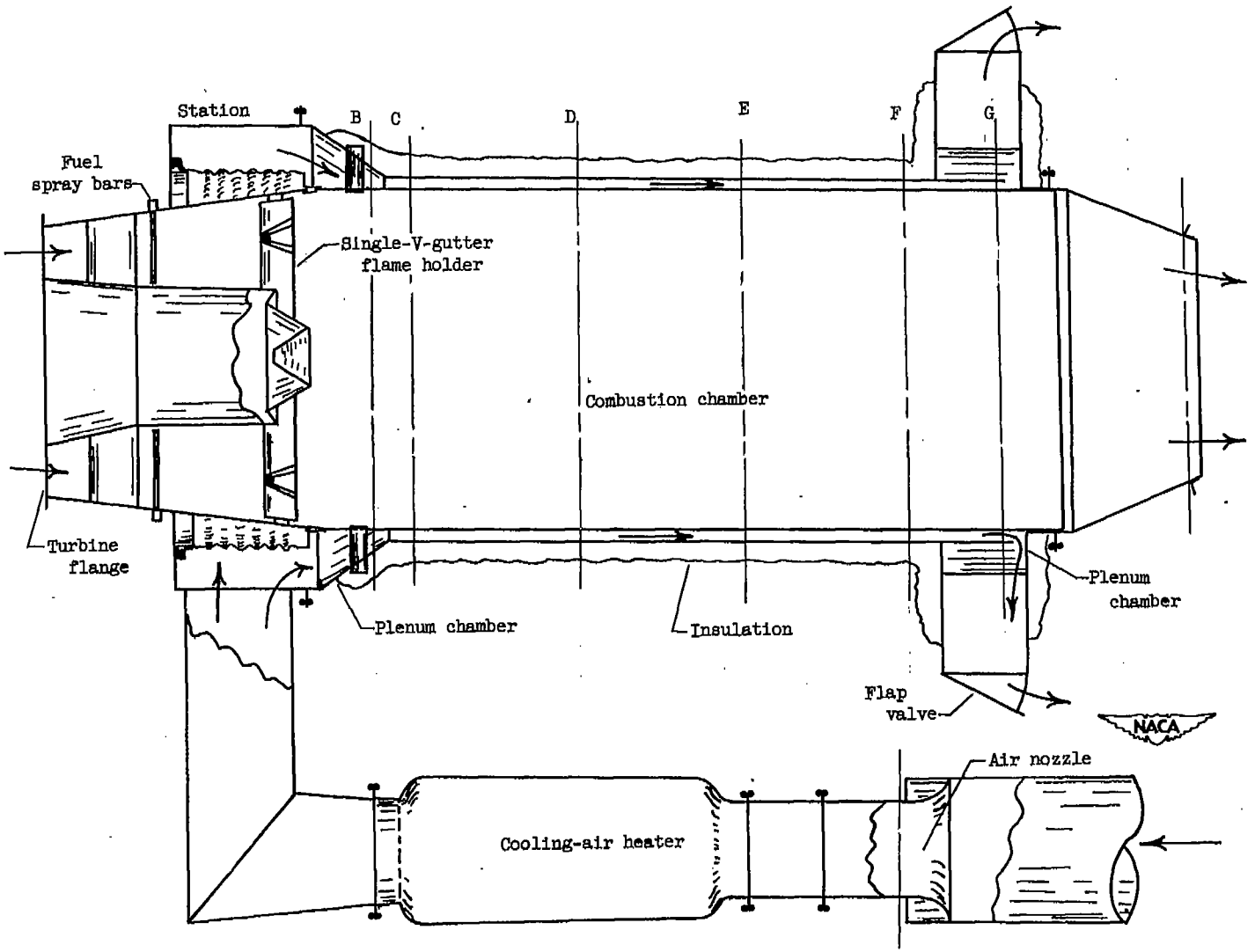

Figure 1. - Schematic diagram of afterburner.

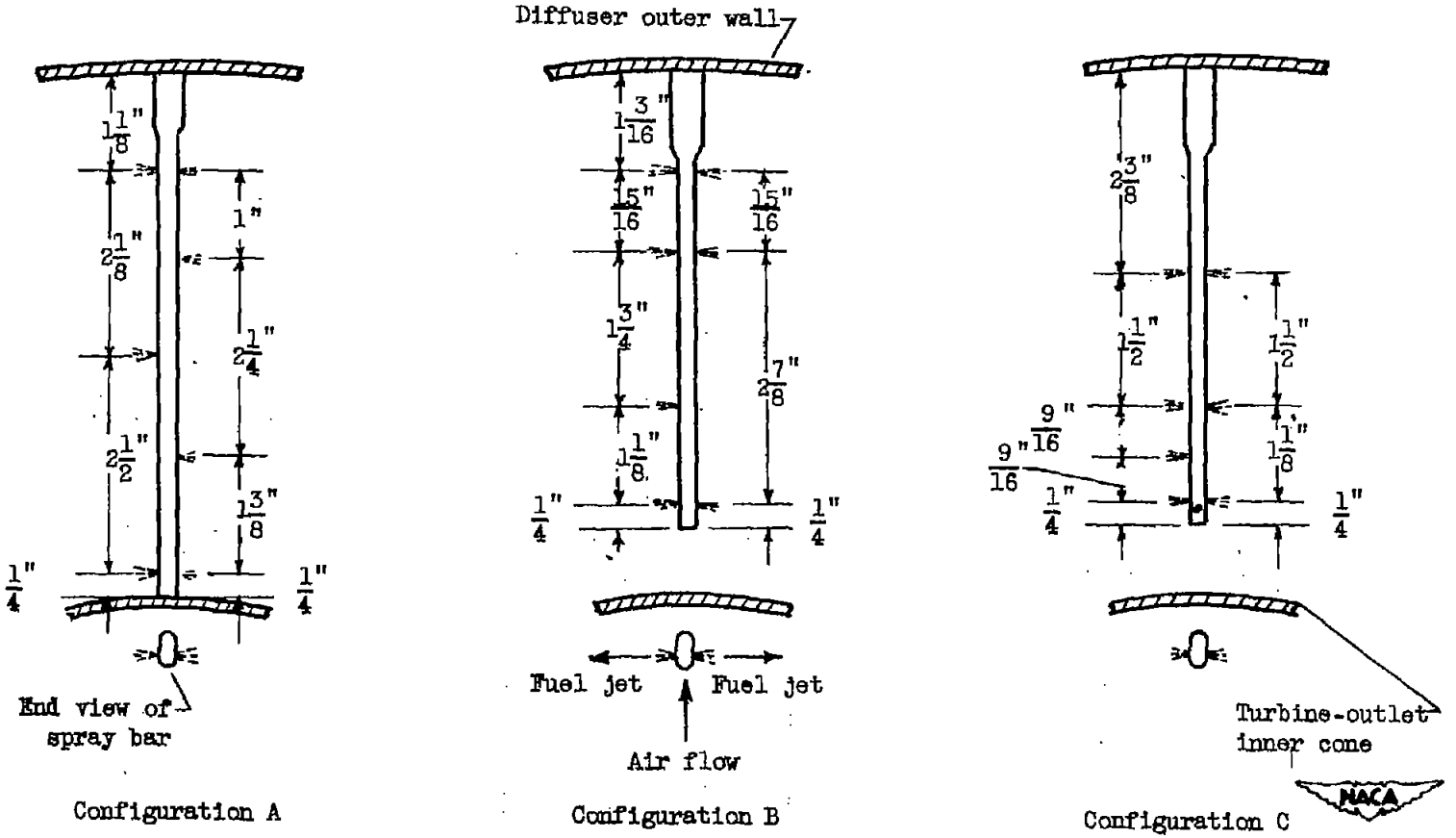

Figure 2. - Downstream view of turbine-outlet annulus showing fuel spray bars for configurations A, B, and C. Diameter of fuel jets, 0.020 inch.

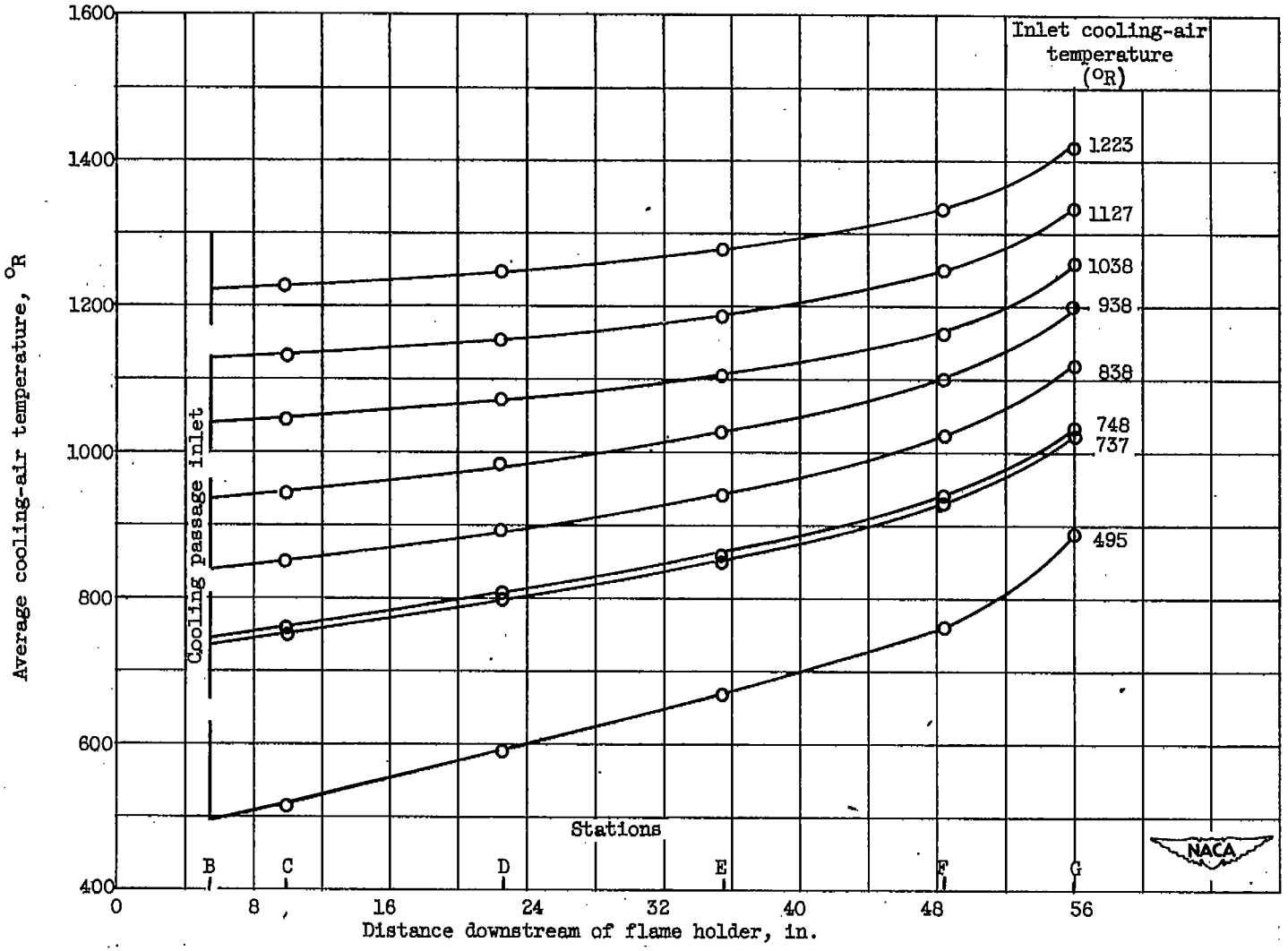

Figure 3. - Longitudinal distribution of cooling-air temperature for several values of inlet cooling-air temperature. Mass-flow ratio, 0.144.

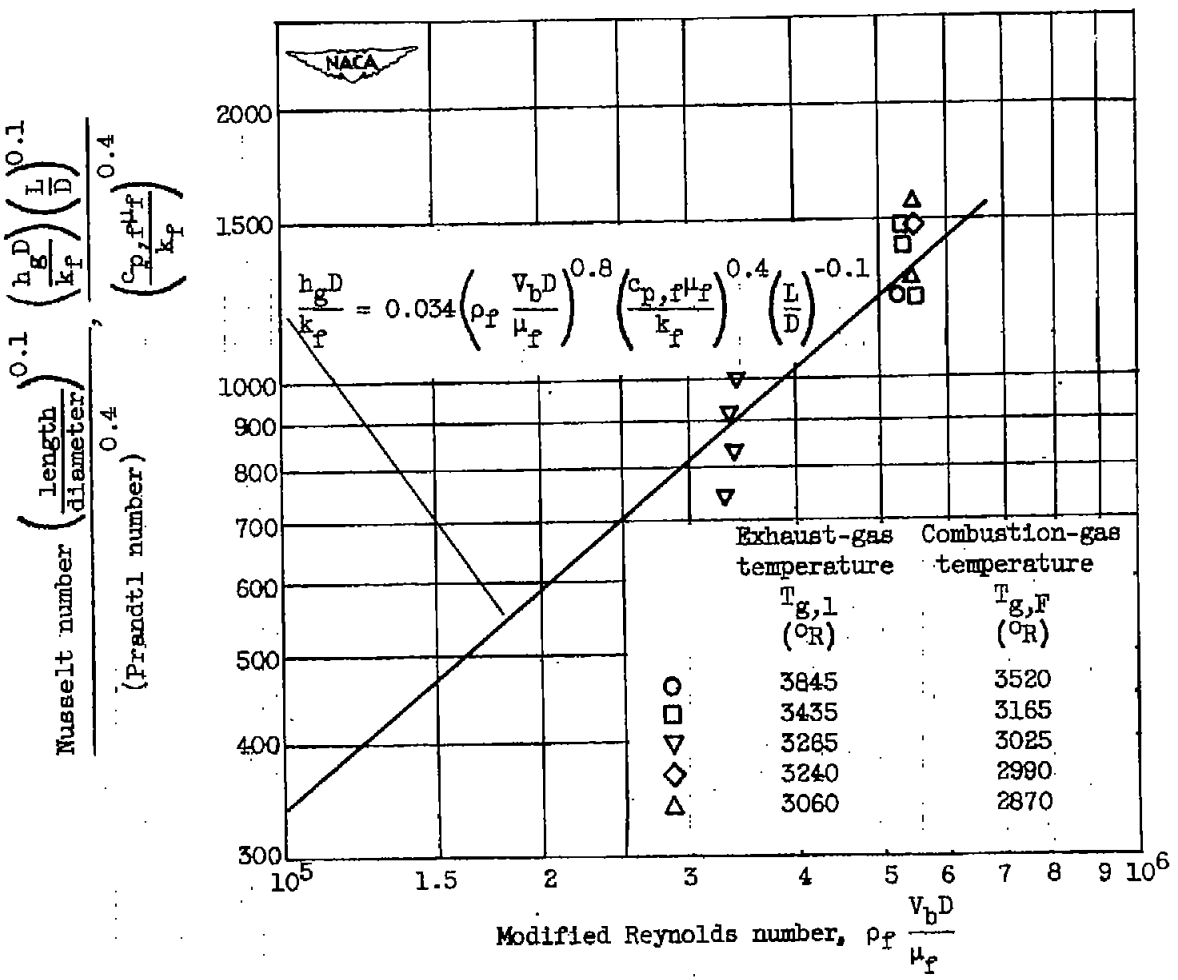

Figure 4. - Correlation of convective heat-transfer coefficient at station F for configuration A. Physical properties of air evaluated at film temperature T_f; thermal conductivity proportional to $\sqrt{T_f}$; average wall temperature $T_{w,F}$, 1510° R.

	Exhaust-gas total temperature T_g (°R)	Mass-flow ratio W_a/W_g	Inlet cooling-air temperature $T_{a,B}$ (°R)	Tail-pipe fuel-air ratio f/a	Average inside wall temperature T_w (°F)	Combustion-gas flow W_g (lb/sec)	Turbine-outlet total pressure (lb/sq ft abs.)
○	2994	0.0672	541	0.0325	1198	21.89	1373
□	2858	.0814	530	.0315	1107	21.98	1350
◇	3306	.1418	1340	.0363	1298	13.61	847
△	3272	.1415	548	.0385	1065	13.78	853
▽	3425	.1411	771	.0450	1158	22.04	1394
◺	3403	.1412	1408	.0444	1401	22.38	1409

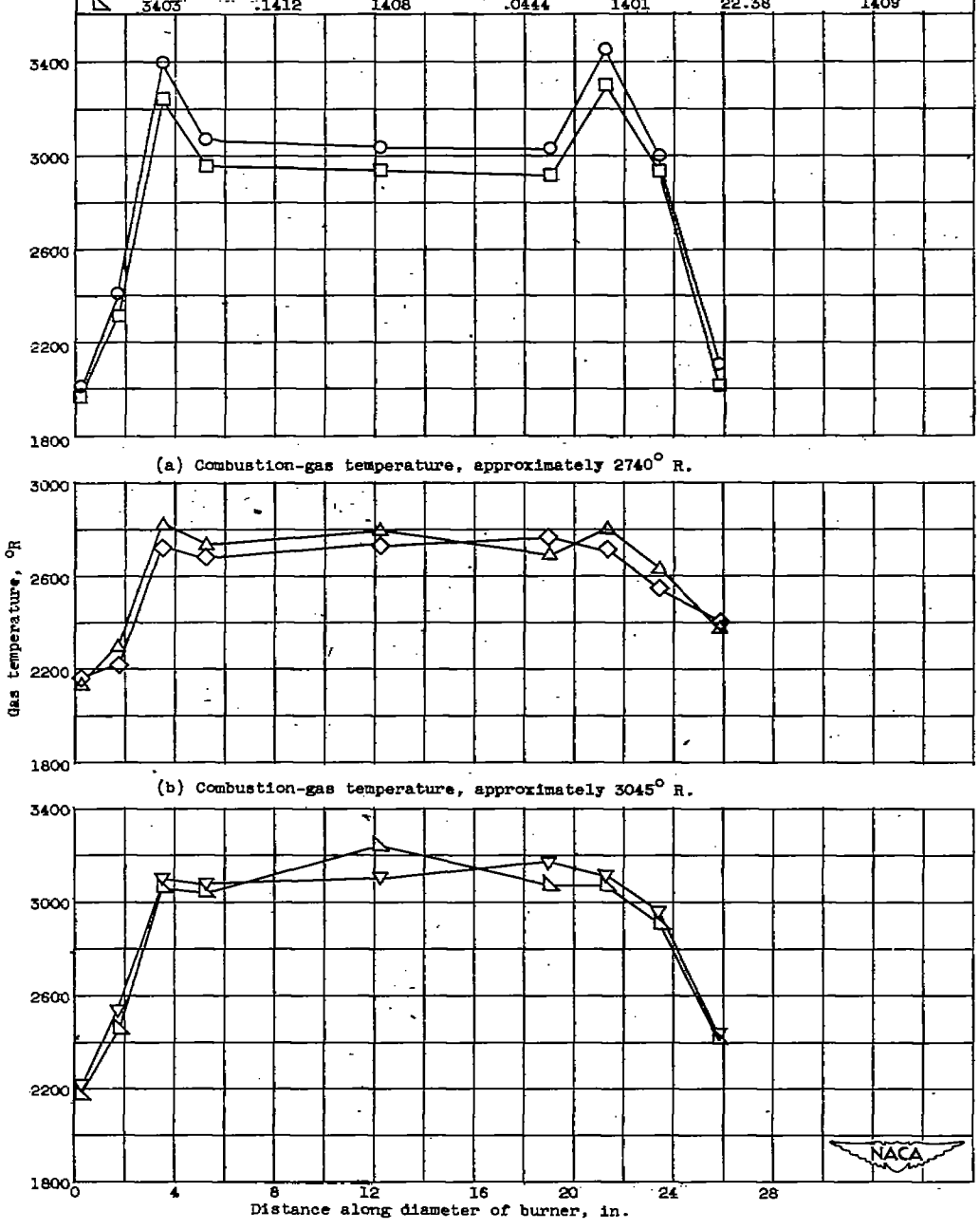

(a) Combustion-gas temperature, approximately 2740° R.

(b) Combustion-gas temperature, approximately 3045° R.

(c) Combustion-gas temperature, approximately 3155° R.

Figure 5. - Transverse profiles of combustion-gas temperature at station F for configuration A.

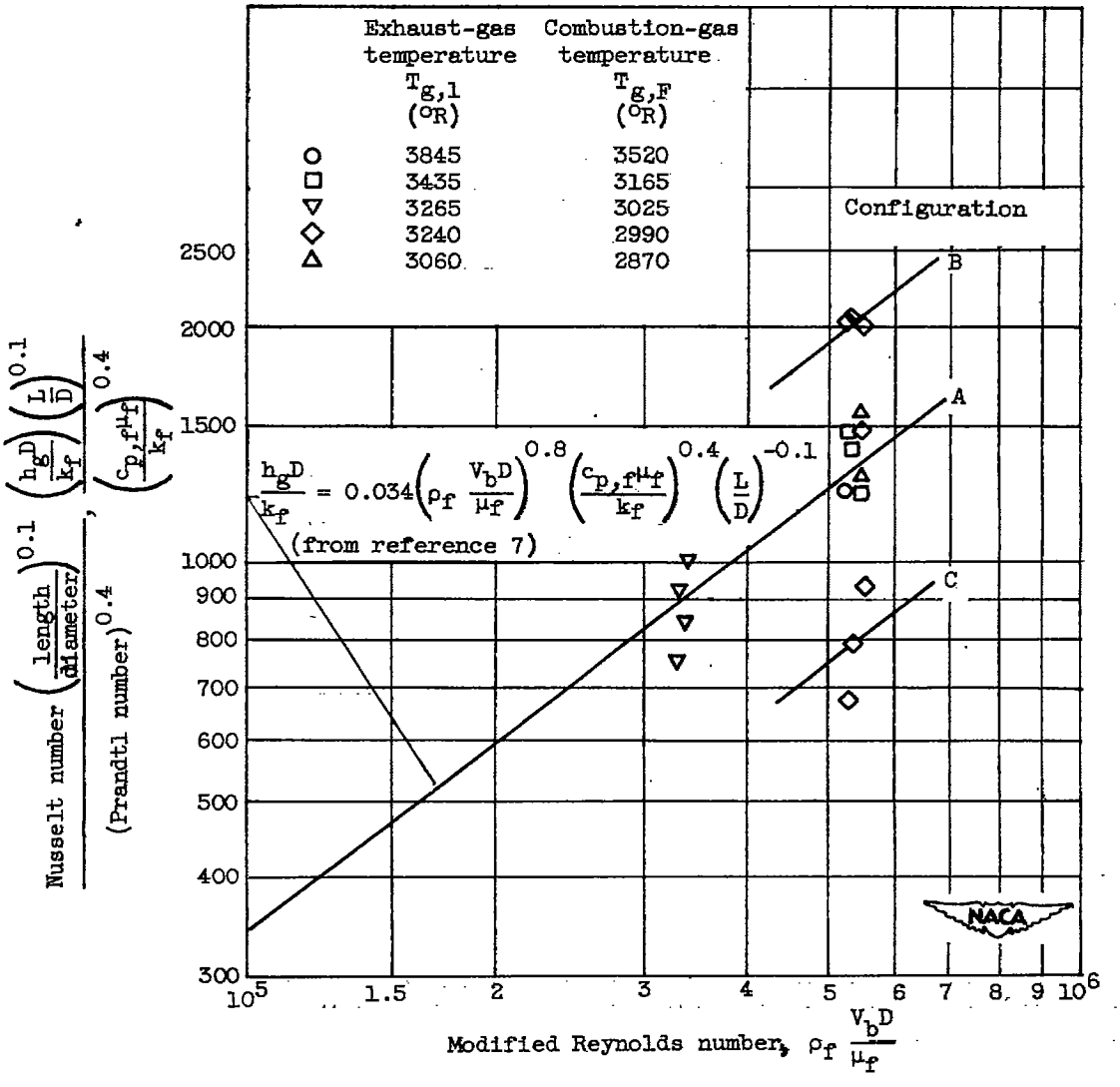

Figure 6. - Correlation of convective heat-transfer coefficient at station F. Physical properties of air evaluated at film temperature T_f; thermal conductivity proportional to $\sqrt{T_f}$; average wall temperature $T_{w,F}$, 1510° R.

2571

	Exhaust-gas total temperature T_g (°R)	Mass-flow ratio W_a/W_g	Inlet cooling air temperature $T_{a,B}$ (°R)	Tail-pipe fuel-air ratio f/a	Average inside-wall temperature T_w (°F)	Combustion-gas flow W_g (lb/sec)	Turbine-outlet total pressure (lb/sq ft abs.)	Average gas temperature 1/4 in. from inside wall $T_{g,1/4}$ (°R)
◇	3305	0.1449	495	0.0409	1164	22.02	1416	2870
◈	3215	.1422	500	.0399	1089	22.23	1410	2840
▽	3214	.1426	828	.0371	999	22.37	1415	2099
◺	3251	.1389	1040	.0370	1096	22.32	1419	2109

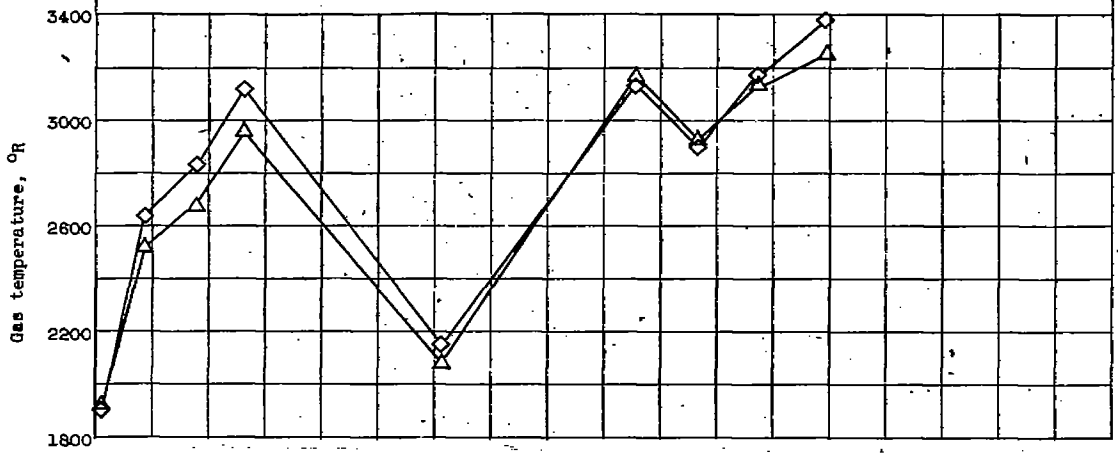

(a) Configuration B.

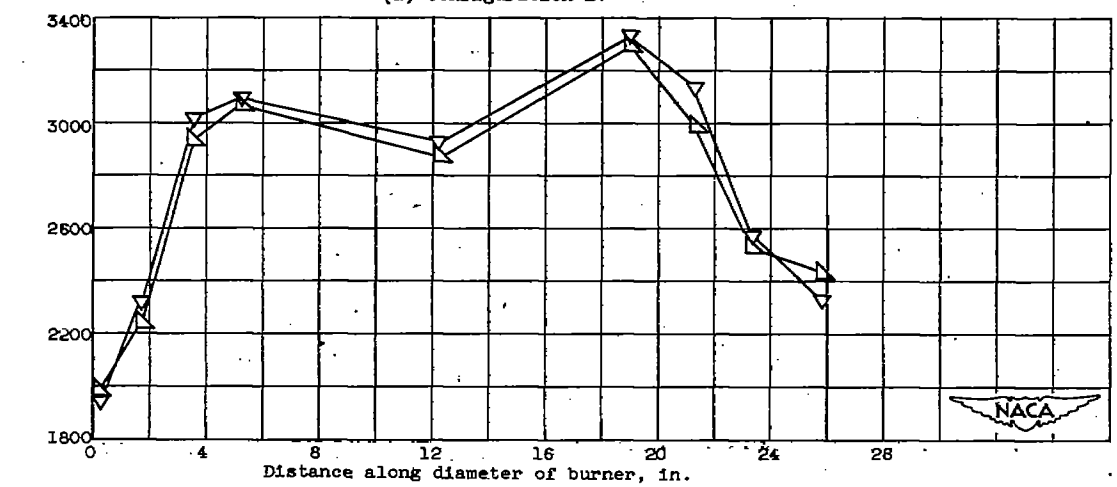

(b) Configuration C.

Figure 7. - Effect of fuel distribution on transverse profiles of combustion-gas temperature at station F; combustion-gas temperature $T_{g,F}$, approximately 3000° R.

[redacted]

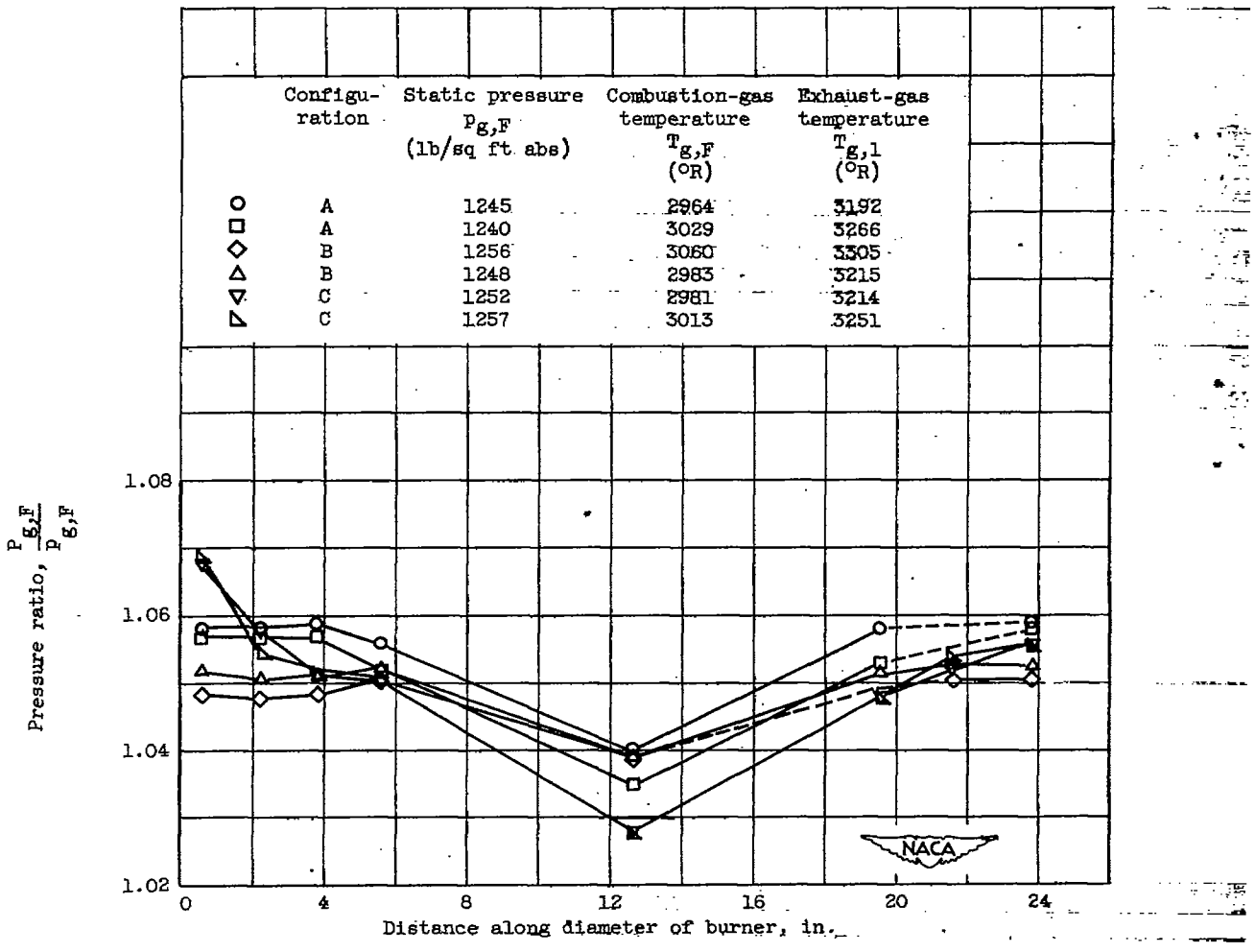

Figure 8. - Transverse profiles of combustion-gas pressure ratio at station F.

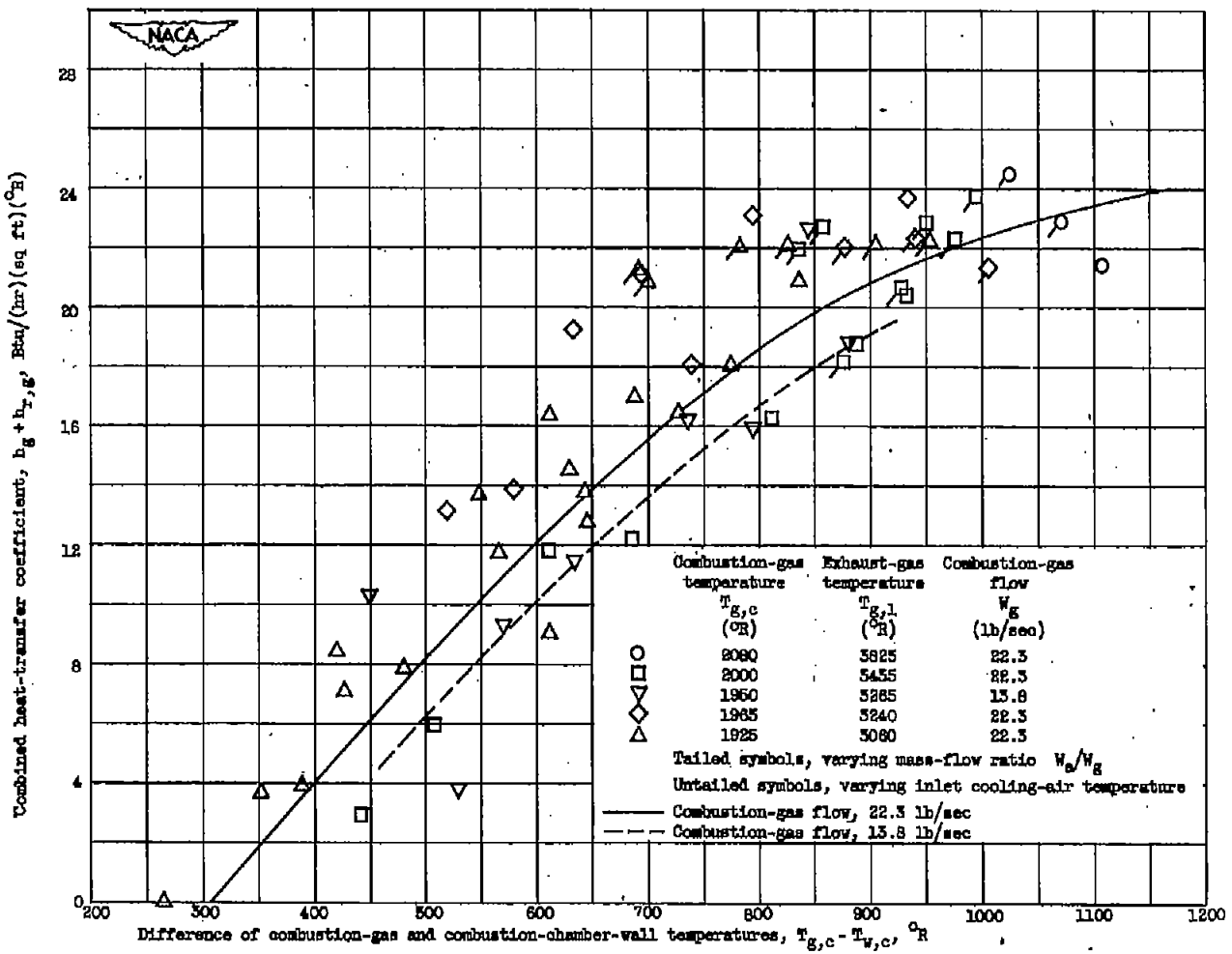

(a) Station C.

Figure 9. - Variation of combined heat-transfer coefficient with difference between temperatures of combustion gas and combustion chamber wall for configuration A.

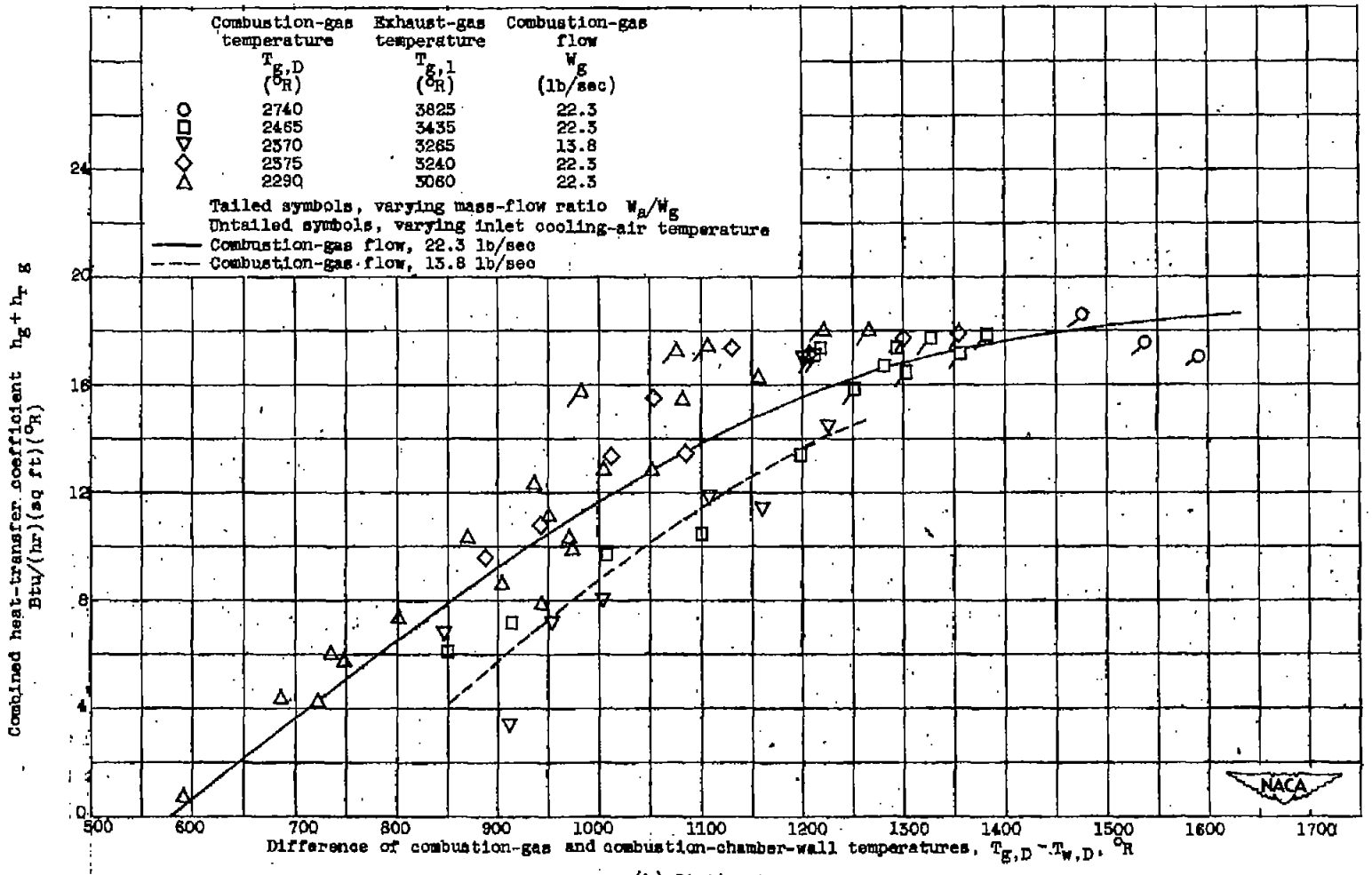

(b) Station D.

Figure 9. - Continued. Variation of combined heat-transfer coefficient with difference between temperatures of combustion gas and combustion chamber wall for configuration A.

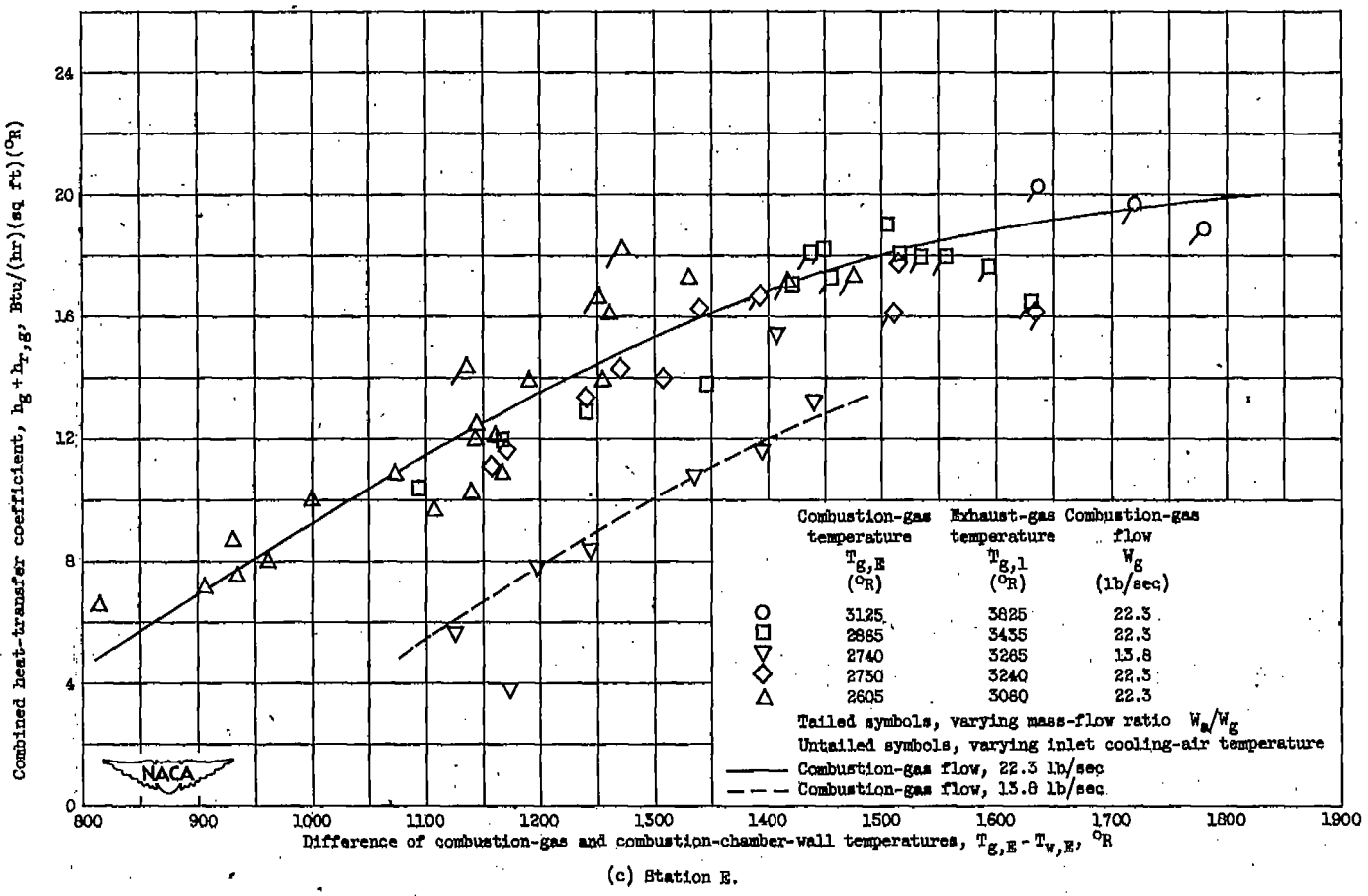

(c) Station E.

Figure 9. - Continued. Variation of combined heat-transfer coefficient with difference between temperatures of combustion gas and combustion chamber wall for configuration A.

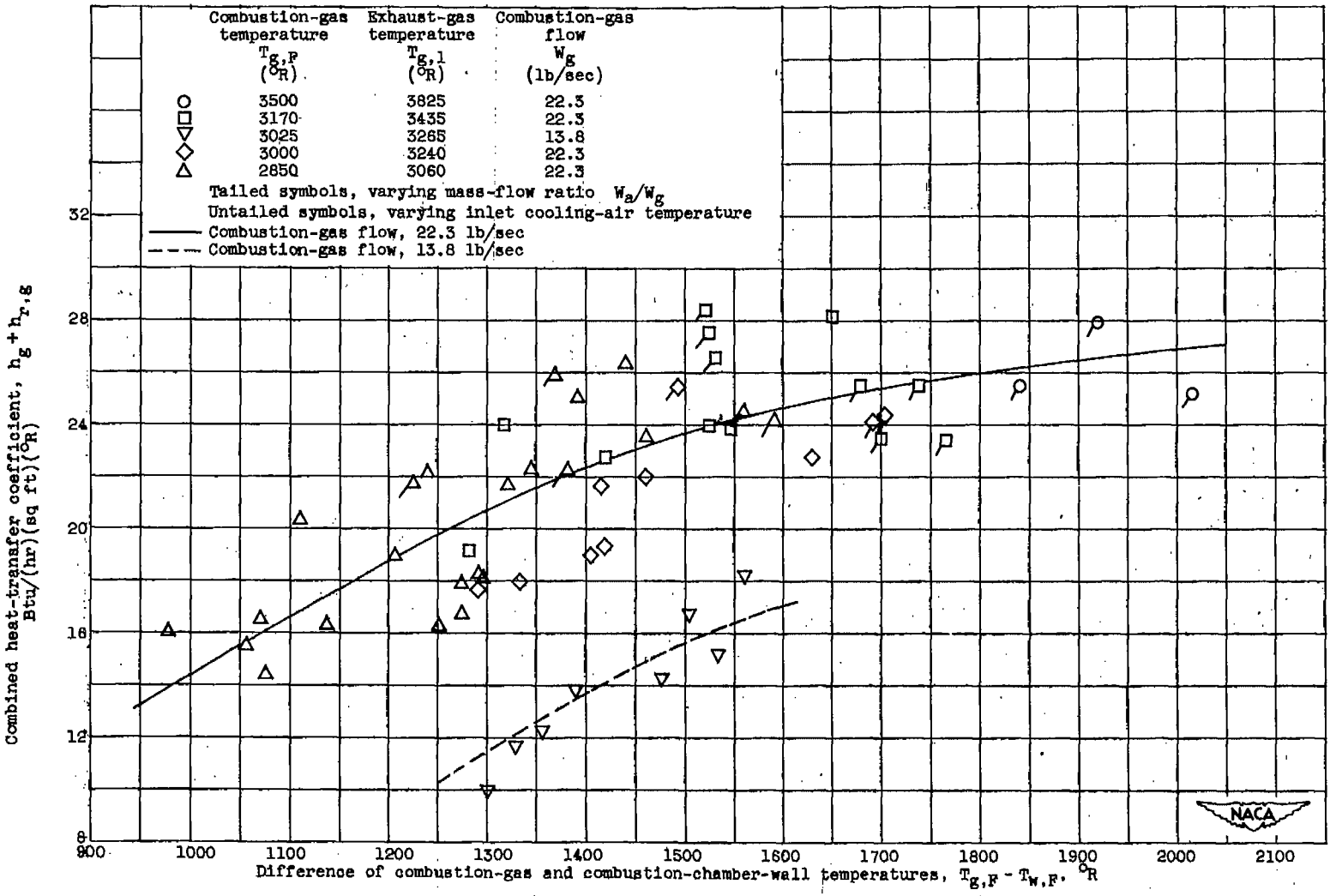

(d) Station F.

Figure 9. - Concluded. Variation of combined heat-transfer coefficient with difference between temperatures of combustion gas and combustion chamber wall for configuration A.

2571

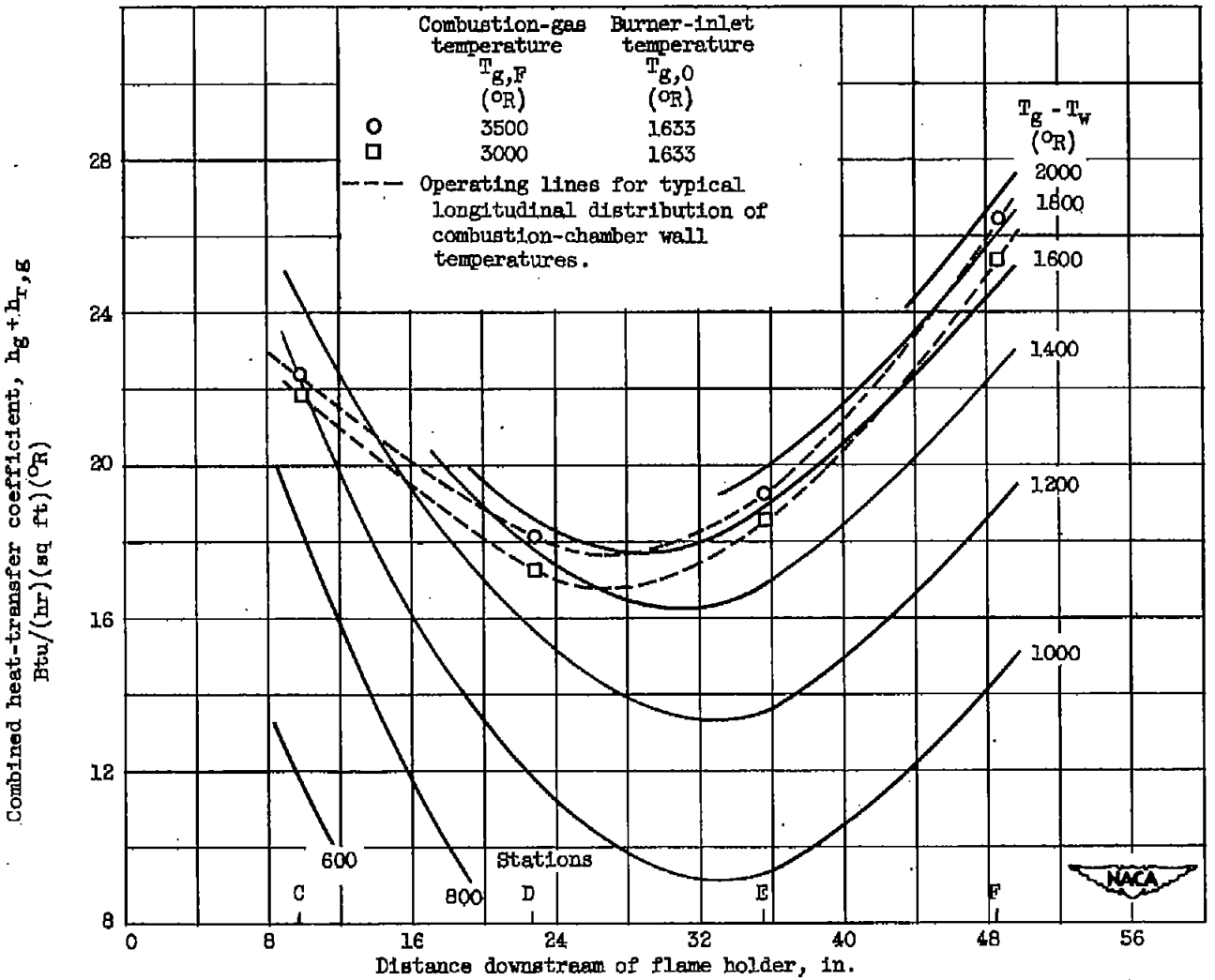

Figure 10. - Variation of combined heat-transfer coefficient with distance downstream of flame holder for configuration A. Combustion-gas flow, 22.3 pounds per second.

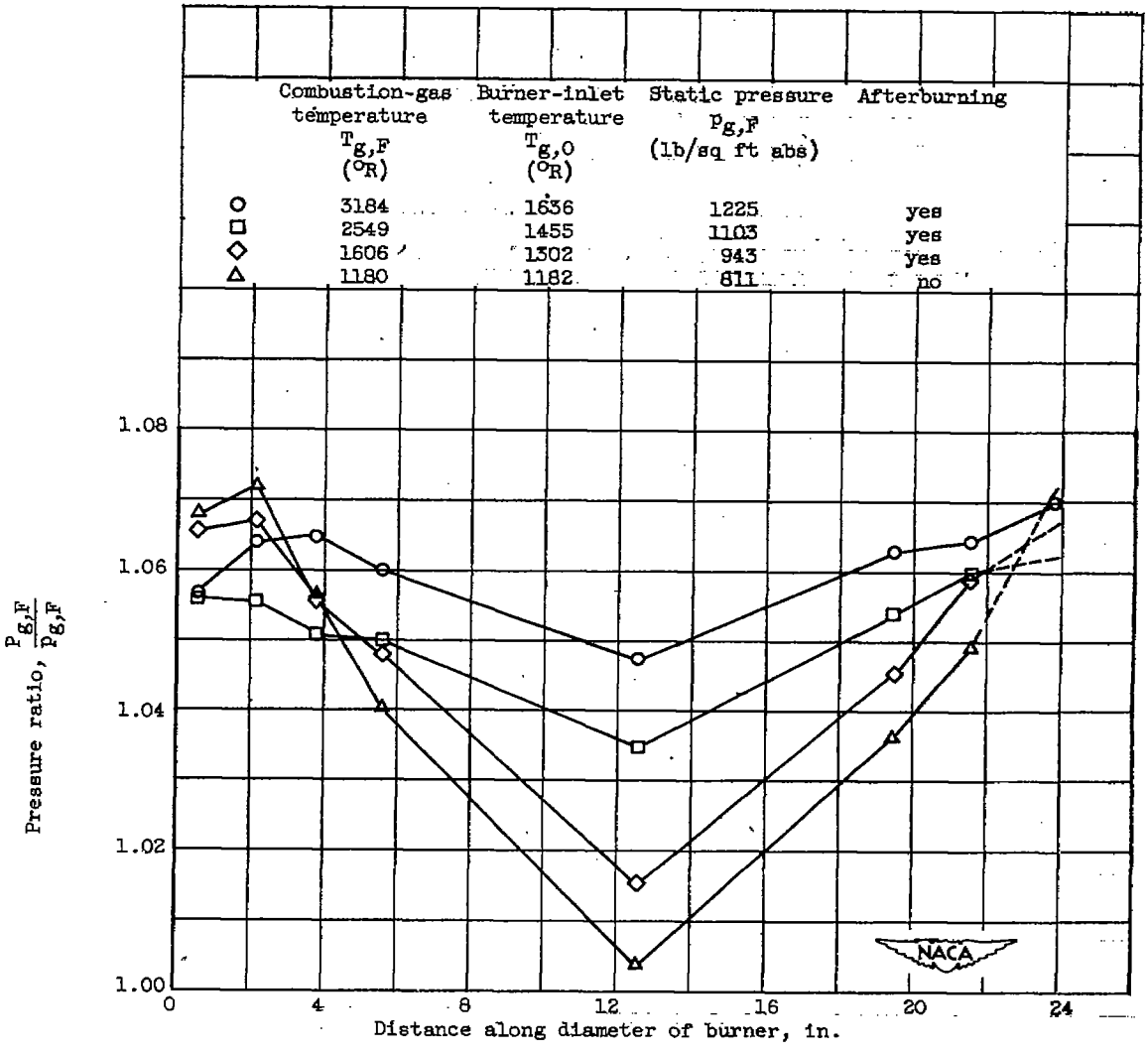

Figure 11. - Variation of transverse profiles of combustion-gas pressure ratio at station F with burner-inlet temperature for configuration A. Combustion-gas flow, 22.3 pounds per second.

2571

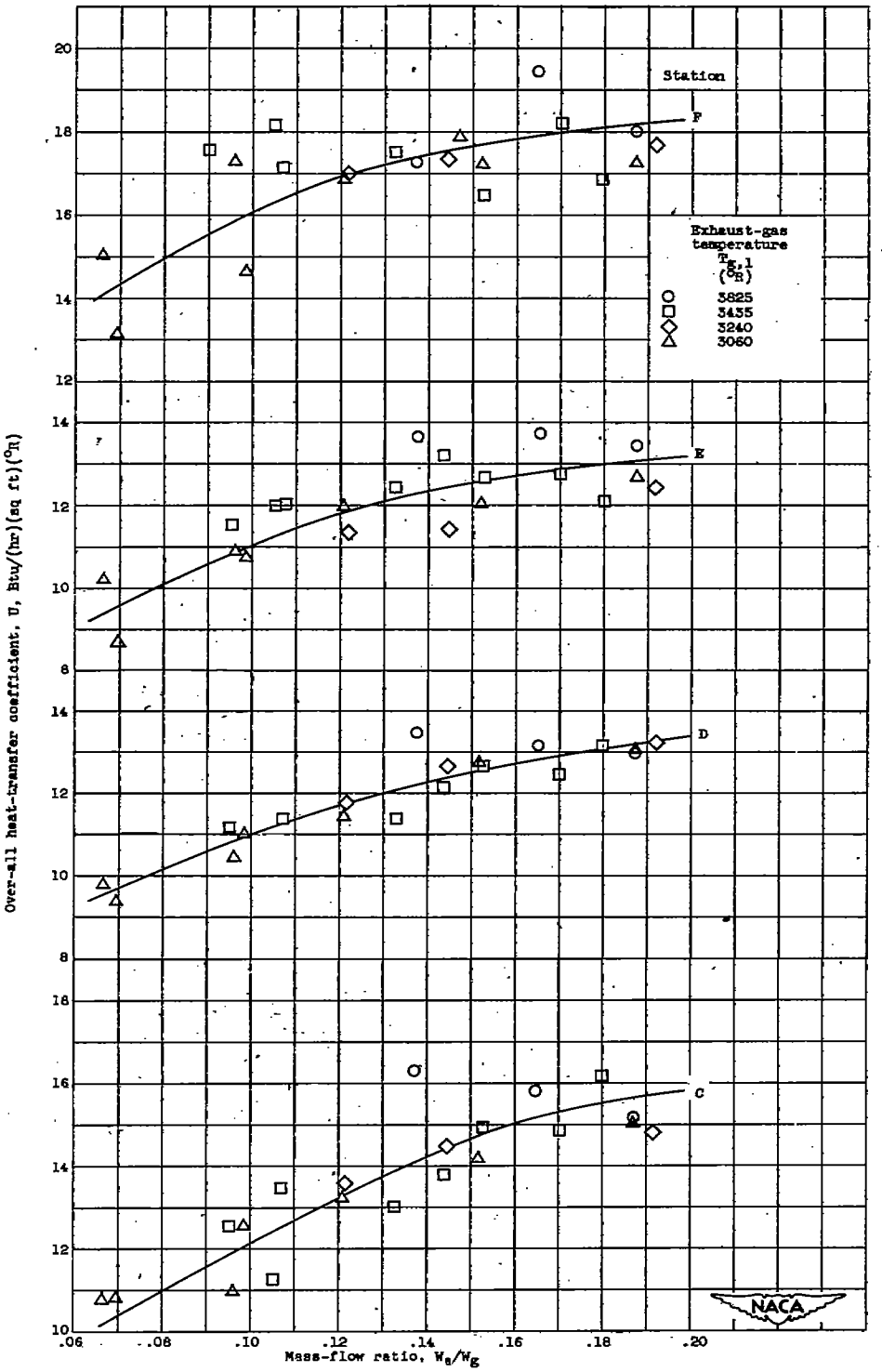

Figure 12. - Variation of over-all heat-transfer coefficient with mass-flow ratio for configuration A. Inlet cooling-air temperature, approximately 520° R; combustion-gas flow, 22.3 pounds per second.

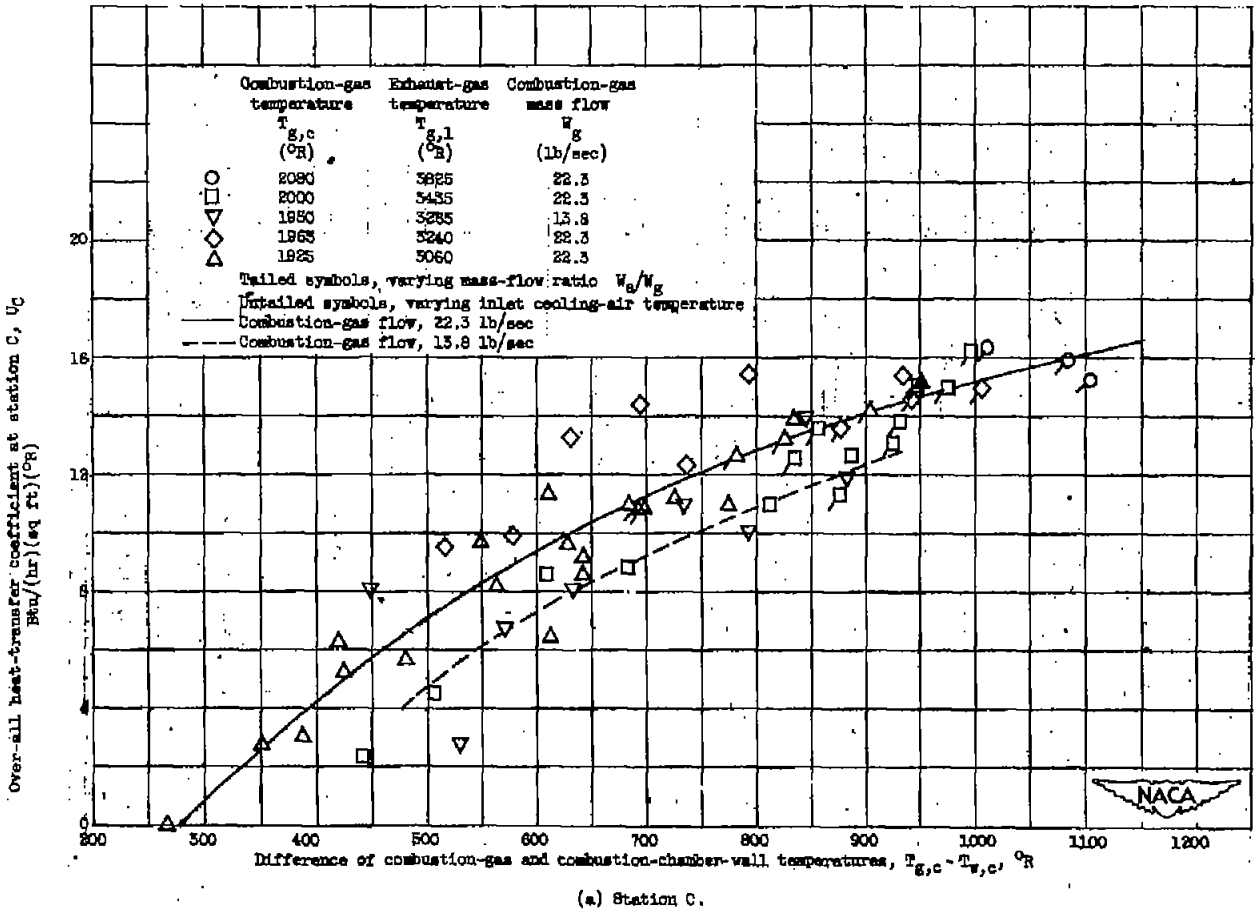

(a) Station C.

Figure 13. - Variation of the over-all heat transfer coefficient with the difference between the temperatures of the combustion gas and combustion chamber wall for configuration A.

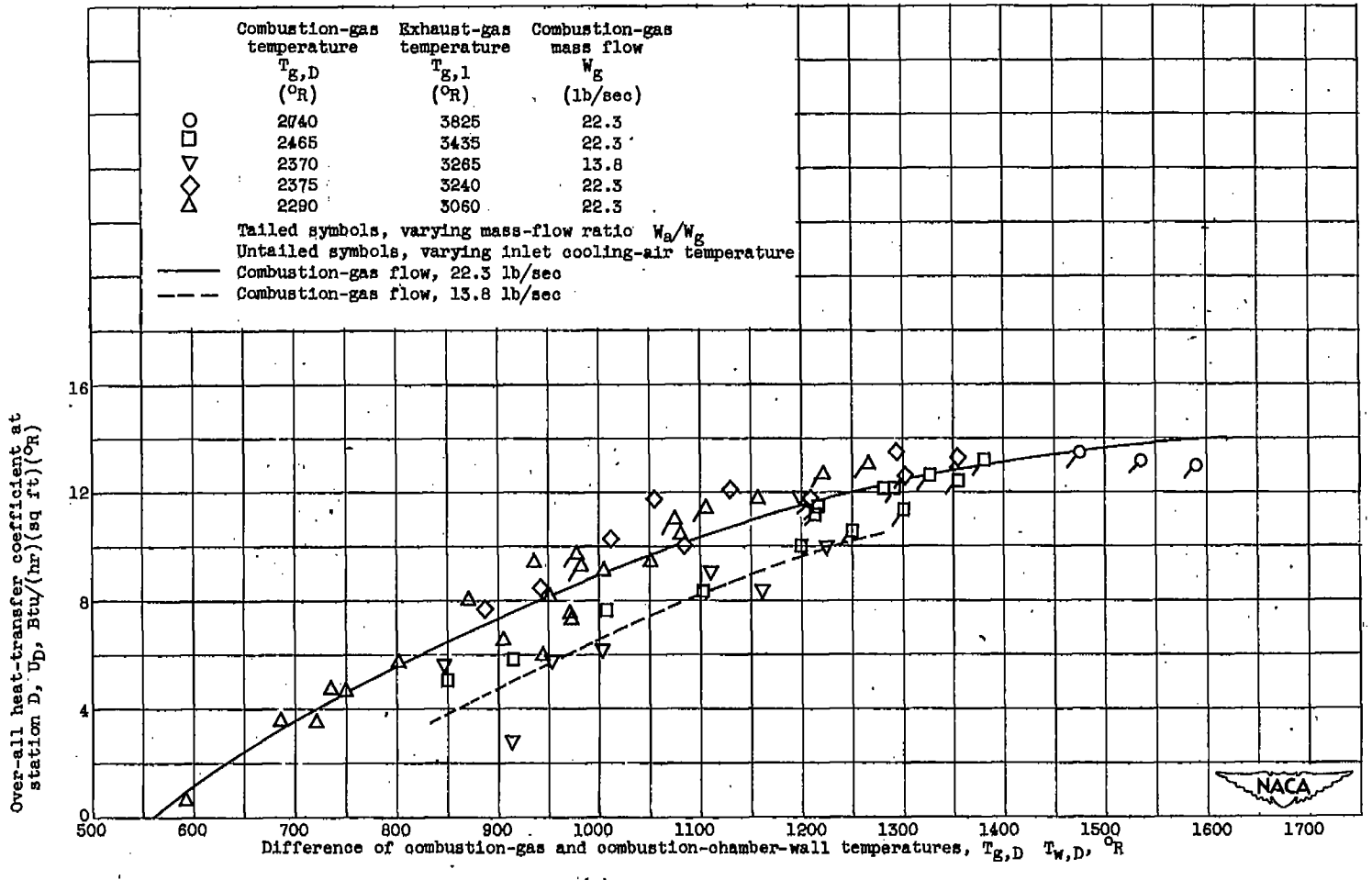

(b) Station D.

Figure 13. - Continued. Variation of the over-all heat transfer coefficient with the difference between the temperatures of the combustion gas and combustion chamber wall for configuration A.

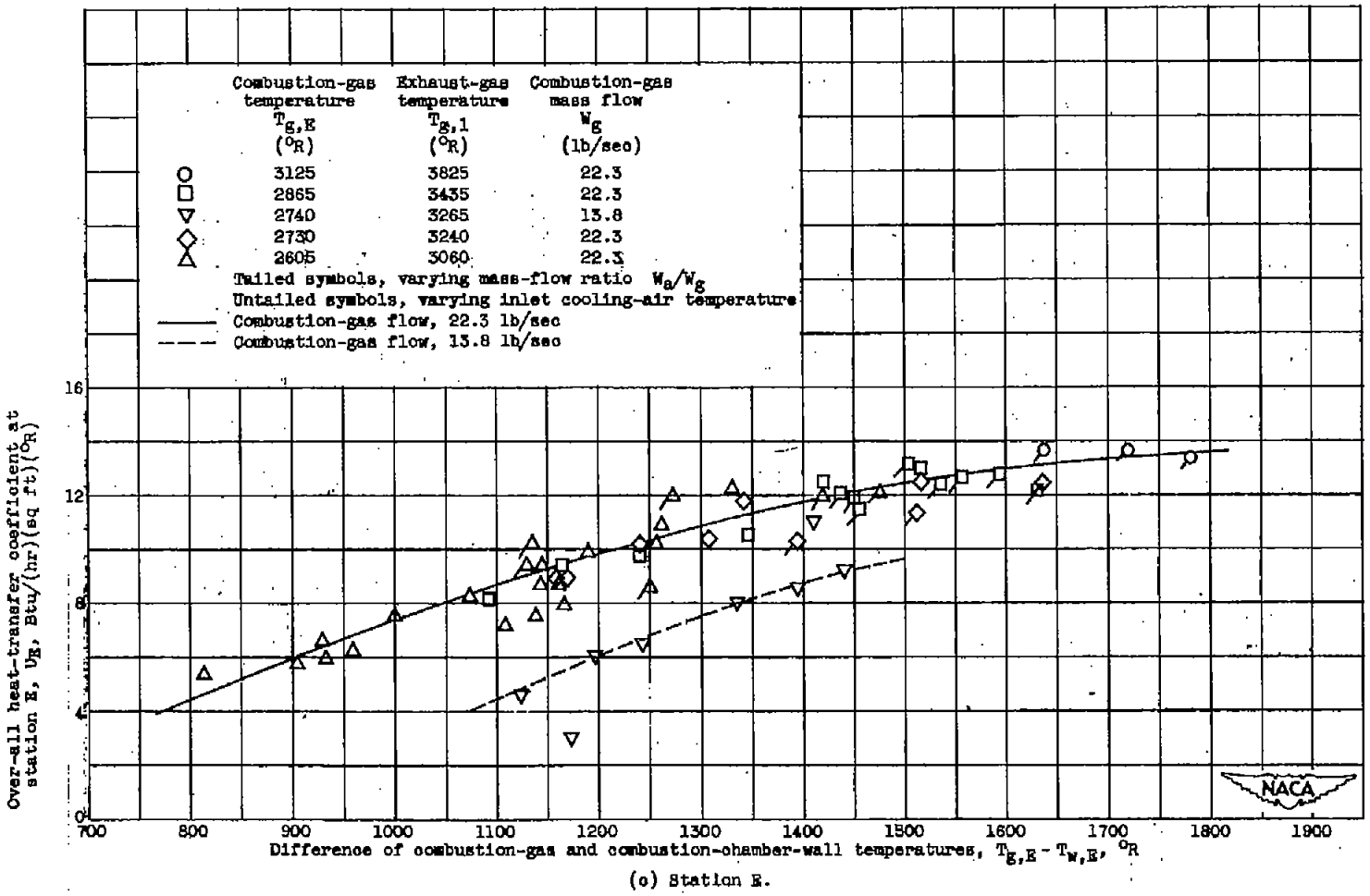

(c) Station E.

Figure 13. - Continued. Variation of the over-all heat transfer coefficient with the difference between the temperatures of the combustion gas and combustion chamber wall for configuration A.

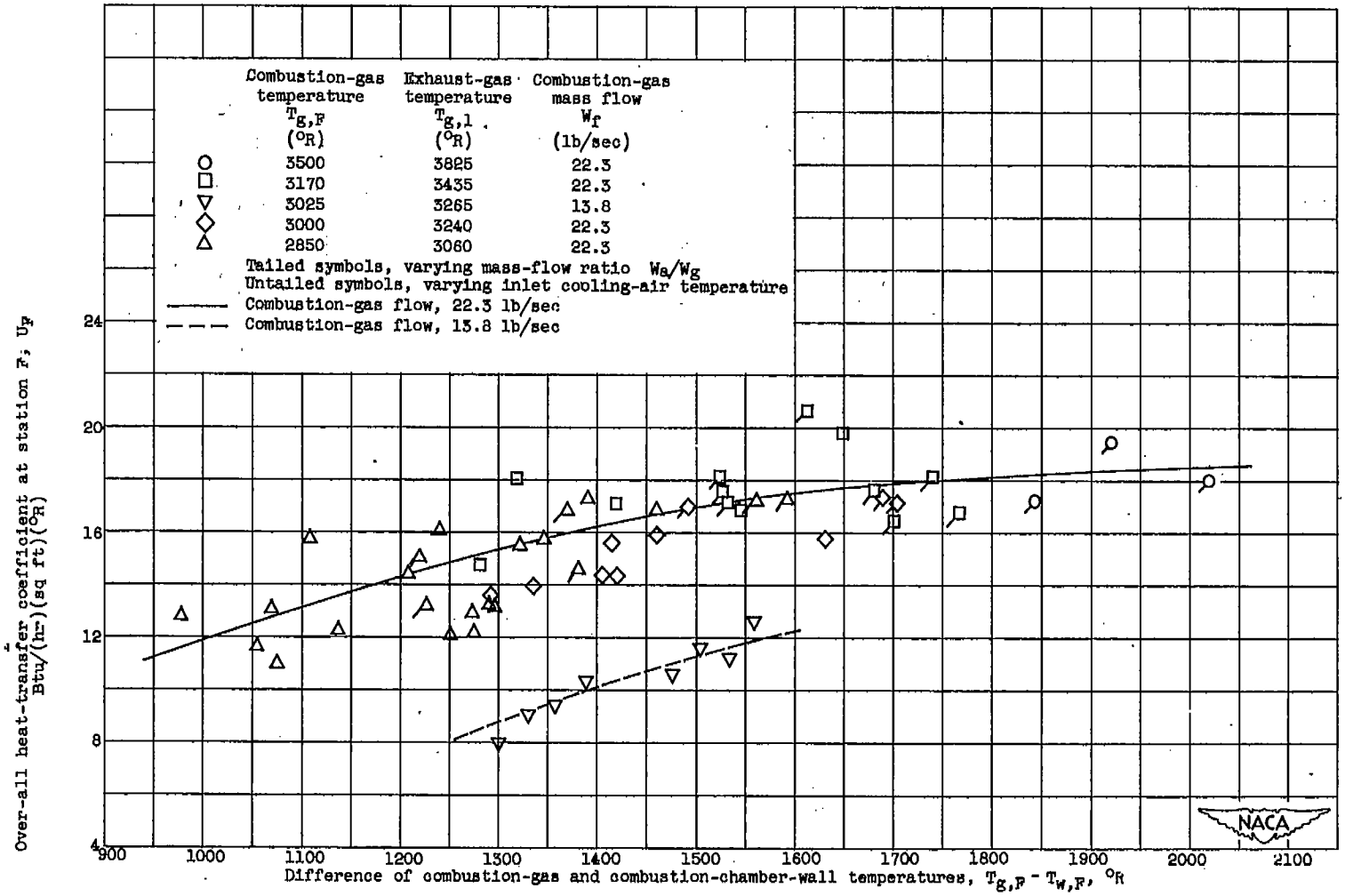

(d) Station F.

Figure 13. - Concluded. Variation of the over-all heat transfer coefficient with the difference between the temperatures of the combustion gas and combustion chamber wall for configuration A.

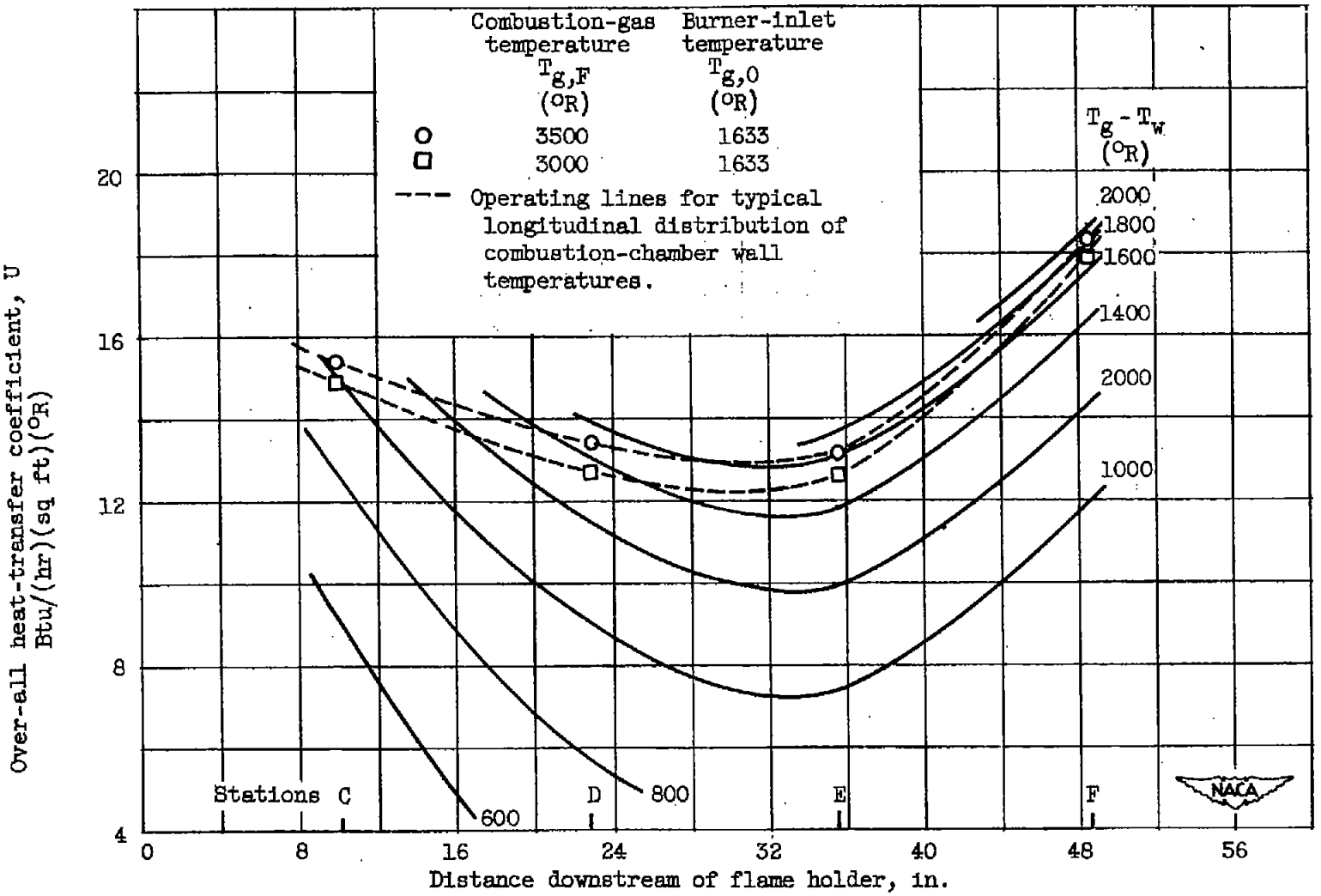

Figure 14. - Variation of over-all heat-transfer coefficient with distance downstream of flame holder for configuration A. Combustion-gas flow, 22.3 pounds per second.

NACA-Langley - 5-21-52 - 496

SECURITY INFORMATION

CONFIDENTIAL

NASA Technical Library
3 1176 01435 5839

CONFIDENTIAL